A mosaic analysis system with Cre or Tomato expression in the mouse

Qun Wang[a], Yen-Yu Lin[a], Baojun Zhang[a], Jianxuan Wu[a], Sumedha Roy[a], Jeremy J. Ratiu[a], Yanping Xu[b], Meifang Dai[a], Laura P. Hale[c], Yue Xiong[b], Qi-Jing Li[a], and Yuan Zhuang[a,1]

[a]Department of Immunology, Duke University Medical Center, Durham, NC 27710; [b]Lineberger Comprehensive Cancer Center, University of North Carolina at Chapel Hill, Chapel Hill, NC 27599; and [c]Department of Pathology, Duke University Medical Center, Durham, NC 27710

Somatic mutations are major genetic contributors to cancers and many other age-related diseases. Many disease-causing somatic mutations can initiate clonal growth prior to the appearance of any disease symptoms, yet experimental models that can be used to examine clonal abnormalities are limited. We describe a mosaic analysis system with Cre or Tomato (MASCOT) for tracking mutant cells and demonstrate its utility for modeling clonal hematopoiesis. MASCOT can be induced to constitutively express either Cre-GFP or Tomato for lineage tracing of a mutant and a reference group of cells simultaneously. We conducted mosaic analysis to assess functions of the *Id3* and/or *Tet2* gene in hematopoietic cell development and clonal hematopoiesis. Using Tomato-positive cells as a reference population, we demonstrated the high sensitivity of this system for detecting cell-intrinsic phenotypes during short-term or long-term tracking of hematopoietic cells. Long-term tracking of *Tet2* mutant or *Tet2/Id3* double-mutant cells in our MASCOT model revealed a dynamic shift from myeloid expansion to lymphoid expansion and subsequent development of lymphoma. This work demonstrates the utility of the MASCOT method in mosaic analysis of single or combined mutations, making the system suitable for modeling somatic mutations identified in humans.

mosaic analysis | *Id3* | *Tet2* | clonal hematopoiesis | lymphoma model

Human genome sequencing has begun to capture the occurrence and progression of somatic mutations in nonpatient populations with increasing detail. For example, clonal hematopoiesis (CH) is now recognized as a phenomenon of clonal expansion driven by acquired mutations in cancer-driver genes in aged but otherwise healthy people (1–4). Recent longitudinal studies of CH involving acute myeloid leukemia (AML) patients have revealed causal links between certain mutations, mostly well-established cancer drivers, and clinical outcomes (5, 6). However, the health impact of most somatic mutations acquired early in life are still incompletely understood. As low cost and deep sequencing links more somatic mutations to CH and clonal expansion in tissues such as skin, liver, and mucosal epithelium (7–10) among asymptomatic people, the need for experimental assessment of the long-term risk of somatic mutations also increases.

Chimeric and mosaic analyses in mice are two main approaches to modeling behaviors of somatic mutations that result in CH. Chimeric mice can be generated by mixing hematopoietic stem cells (HSC) from wild-type and mutant strains during adoptive transfer to lethally irradiated hosts. This approach is highly effective in demonstrating clonal advantage and transformation of HSC harboring designated cancer mutations (11, 12), but is less ideal for simulating the human CH that is detected at low frequency in healthy individuals. Mosaic analysis represents an alternative approach to modeling CH. Without disrupting the immune system, induction of genetic mosaicism in the mouse enables lineage tracing of mutant cells in an otherwise wild-type background. The Cre/loxP-based induction of mosaicism has been used in the study of CH when the Cre activity is limited to a fraction of hematopoietic cells either in a regulated

(13) or a fortuitous (14) manner. By coupling with an independent reporter, the inducible CreER and MxCre systems (15, 16) have been broadly used as an effective tool in the study of clonal expansion driven by single mutations. However, quantitative tracking of a small number of mutant cells during the early phase of CH remains difficult in the absence of an internal control.

Mosaic analysis tools, such as MADM (mosaic analysis with double markers) (17) and MASTR (mosaic mutant analysis with spatial and temporal control of recombination) (18), have been developed to enable tracking of conditionally induced mutations with lineage markers. The MADM system allows the generation of differentially labeled daughter cells from mitosis for side by side comparison of mutant and wild-type cells (17). Because the design is based on mitotic recombination between paired chromosomes, the MADM system and other similar designs (19) are limited to studies of genes linked with the reporter on the same chromosome (20, 21). The MASTR method uses an inducible Flp recombination system to constitutively activate Cre (18), which allows simultaneous deletion of a conditional targeting allele and activation of a lineage marker within the same cells. Although the MASTR system can be applied to the study of any conditional allele on any chromosomes, quantification of the mutant clones is challenging due to the lack of an internal reference population. Thus far, uses of the MADM and MASTR systems in CH studies have not been reported.

We developed a mosaic analysis system with Cre or Tomato, named MASCOT. This reporter system produces differentially labeled mutant and wild-type cells from any Cre/loxP-based conditional alleles in the mouse. We then tested the utility of MASCOT in the study of hematopoiesis and CH. First, we

Significance

Somatic mutations are the driving force of many age-related diseases such as cancer and hematopoietic failure. A challenge in the field is to evaluate health impact of somatic mutations prior to the appearance of disease symptoms. We describe a genetic tool named MASCOT (mosaic analysis system with Cre or Tomato) for mosaic analysis of somatic mutations that drive clonal hematopoiesis and lymphomagenesis. MASCOT can be applied to mosaic analysis of broad tissue types, and thus provides a valuable tool to aid functional dissection of somatic mutations in studies of development and disease.

validated the MASCOT system in mosaic analysis of ID3, a transcription regulator with well-characterized roles in lymphopoiesis (22). Mosaic analysis of MASCOT not only confirmed cell-intrinsic roles of ID3 in regulating lymphopoiesis but also revealed a function of ID3 for regulating long-term homeostasis of colonic macrophages. Second, we used the MASCOT method to track the generation and long-term progression of CH induced by deletion of the Ten Eleven Translocation 2 (*Tet2*) gene (23). We found that CH induced by *Tet2* deletion promoted myeloid expansion resembling clonal hematopoiesis of indeterminate potential (CHIP) (24). Third, we carried out mosaic analysis of *Tet2/Id3* double mutations and revealed a strong impairment in lymphopoiesis caused by concurrent deletion of

Tet and *Id3*. Fourth, the long-term tracking of mosaic mice revealed development of *Tet2*-deficient lymphoma, making the mosaic mice a model for studying the transition from CHIP to lymphoma. These proof-of-principle studies demonstrate that MASCOT is an effective tool for modeling CH and for functional dissection of somatic mutations relevant to human diseases.

Results

Construction of MASCOT Reporter Mice. In building a mosaic analysis system for tracking somatic mutations, we sought to satisfy three basic criteria: 1) Somatic mutations can be induced in any tissues at low frequency by tamoxifen treatment. 2) Both mutant and wild-type reference populations are generated concurrently and
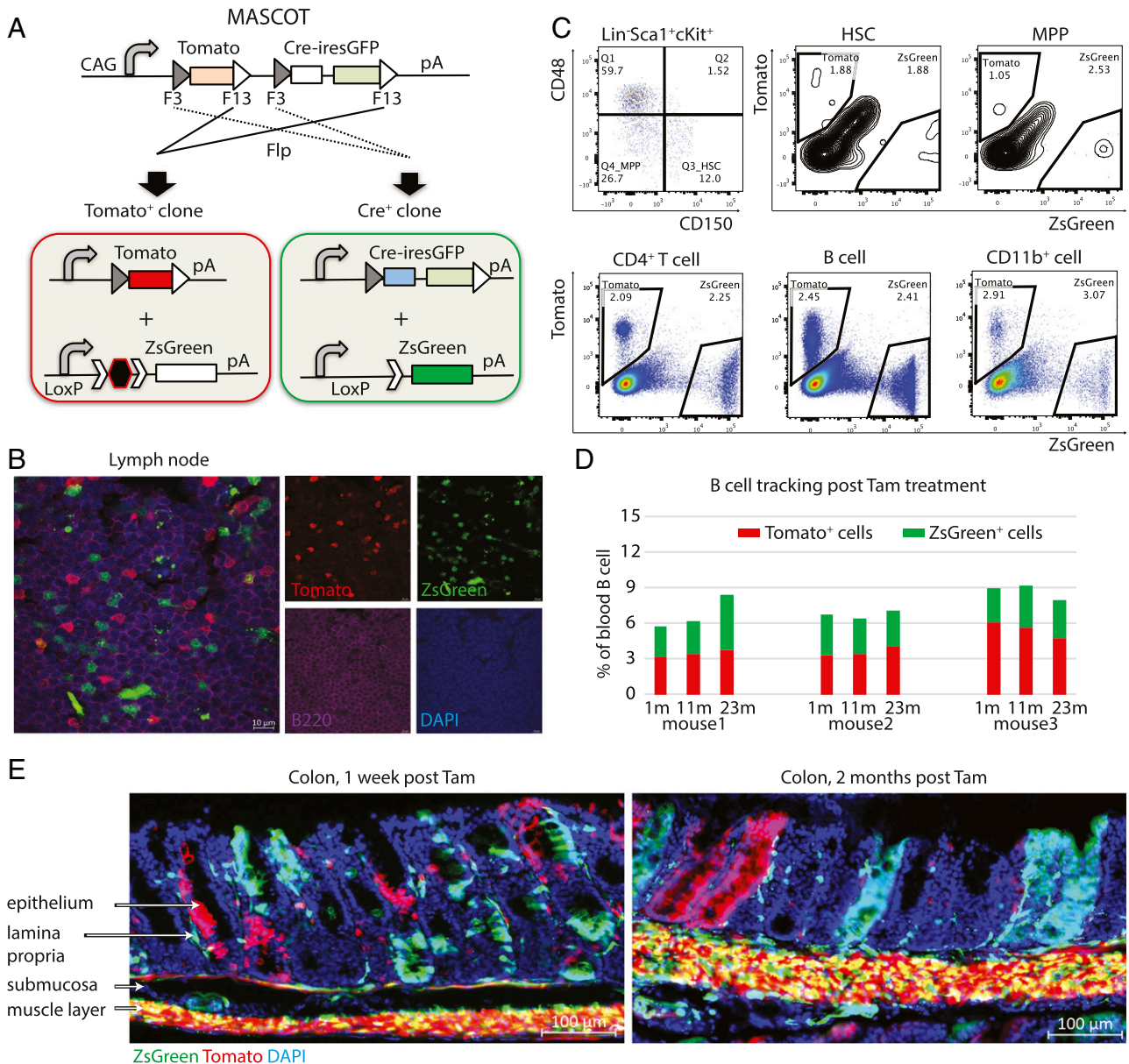

Fig. 1. Generation and lineage tracking of mosaic clones with the MASCOT method. (*A*) Key elements of the MASCOT reporter and its binary outcomes after Flp/FRT-mediated recombination. A separate *R26^ZsGreen* reporter was included to aid detection of Cre-expressing cells. (*B*) Detection of Tomato and ZsGreen fluorescent signals by four-color fluorescent microscopy of a lymph node section. B220 and DAPI staining mark B cells and nuclei, respectively. (*C*) FACS analysis of mosaicism in HSC, MPP, T, B, and myeloid cells. Data are from a single mouse, representing seven tested. (*D*) Longitudinal lineage tracking of Tomato- and ZsGreen-positive B cells in blood over 23 mo of three mice with mosaicism induced at the weaning age. (*E*) Fluorescent microscopy of frozen sections of colon tissues from *Cot2/Cot2;R26^F/Z* mice at 1 wk (*Left*) or 2 mo (*Right*) posttamoxifen treatment. Images are native fluorescent signals from the ZsGreen and Tomato markers with DAPI staining of nuclei on frozen sections. Results shown are representative of three mice in each treatment group.

tagged with distinct lineage markers for lineage tracing. 3) The method must be applicable to the study of any single mutation or compound mutations by crossing to preexisting conditional alleles. With these design principles in mind, we have established the MASCOT reporter (Fig. 1A). This reporter contains the CAG (CMV enhancer chicken beta Actin promoter beta-Globin first intron) promoter, which drives constitutive expression of either the Tomato marker or the Cre recombinase upon Flp/FRT-mediated recombination. The Cre cDNA is tagged at its 3′ end with iresGFP for lineage tracing of Cre expression. The Tomato and Cre coding sequences are flanked by two distinct pairs of FRT sites (25) with the internal FRT sites hopping over each other. Although the entire reporter is constitutively transcribed by the CAG promoter, Cre translation is disrupted by the preceding translational stop of the Tomato cassette. Flp-induced recombination between either of the FRT pairs results in deletion of either Tomato or the Cre-GFP cassette, resulting in mutually exclusive expression of either Cre-GFP or Tomato, respectively. We tested the construct in 3T3 cells and confirmed Flp-dependent conversion from Tomato/GFP double-positive to Tomato or GFP single-positive clones (*SI Appendix*, Fig. S1A). We found that Tomato expression is enhanced upon deletion of the Cre-GFP cassette [presumably due to elimination of nonsense-mediated RNA decay (26)], whereas the level of GFP expression remains the same. In the subsequent in vivo studies, we used a ZsGreen reporter, which is much brighter than GFP, to track Cre activity (*SI Appendix*, Fig. S2A).

We introduced the reporter cassette into the mouse genome as a *piggyBac* transposon to produce single-copy transgenic lines (27). To select single-copy integration events outside any essential genes, we crossed the founder mouse to a *piggyBac* transposase expression strain and screened for new insertion events in the F2 generation (*SI Appendix*, Fig. S1B). The low-level expression of Tomato from the reporter in blood cells facilitated easy identification of transposon carriers among the progeny for further characterization. Three independent insertional events on separate chromosomes were identified through inverse-PCR mapping. All three lines displayed similar reporter activities in response to tamoxifen treatment. Based on lack of any overt phenotypes and normal breeding performance, we

chose to maintain the insertion allele on chromosome 2 and named the allele as *Cot2*, for Cre or Tomato on chromosome 2 for subsequent studies (*SI Appendix*, Fig. S1 C and D). Similar to what we found in 3T3 cells, the mosaic reporter supports low-level expression of Tomato and GFP, a convenient feature that can be used in tracking the *Cot2* allele during breeding (*SI Appendix*, Fig. S1E). We then bred the *Cot2* line with the $R26^{FlpoER}$ strain (or $R26^F$) (18) and a modified version of the $R26^{ZsGreen}$ strain (or $R26^Z$, *Materials and Methods*) (28), which provide a tamoxifen-inducible Flp recombinase and a Cre-dependent ZsGreen reporter, respectively (*SI Appendix*, Fig. S2A). Tamoxifen treatment of $Cot2/+;R26^{F/Z}$ mice yielded Tomato-positive and ZsGreen-positive cells that were readily detectable by fluorescent microscopy (Fig. 1B) and flow cytometry (Fig. 1 C and D). Staining with lineage markers confirmed mosaic patterns in multiple cell lineages including HSC, multipotent myeloid progenitors, myeloid, T, and B cells (Fig. 1C). To determine the range of labeling efficiency with the *Cot2* reporter in blood cells, we tested varying doses of tamoxifen treatment of $Cot2/Cot;R26^{F/Z}$ mice (*SI Appendix*, Fig. S2 B–D). With one round of intraperitoneal delivery of tamoxifen, we typically obtained less than 5% of lineage-labeled cells. However, with three rounds of tamoxifen treatment, we observed up to 20–30% of lineage-labeled cells in the hematopoietic compartment. Among lineage-labeled cells, Tomato$^+$/ZsGreen$^+$ double-positive cells were also detected with expected frequency (assuming *Cot2* on homologous chromosomes are independently activated, *SI Appendix*, Fig. S2D). The frequencies of Tomato$^+$ and ZsGreen$^+$ single-positive cells were close to equal, even though there were variations among the individual mice treated under the same condition (*SI Appendix*, Fig. S2C). Periodic blood tests demonstrated persistence of the mosaic patterns in the blood throughout the normal lifespan of the mouse, confirming long-term stability of mosaic clones that were established in HSC by tamoxifen treatment at a young age (Fig. 1D and *SI Appendix*, Fig. S2E).

Mosaicism was also established in nonhematopoietic compartments such as colonic muscle and epithelium (Fig. 1E and *SI Appendix*, Fig. S2F). Colonic epithelium is made of individual crypts that undergo constant regeneration from stem cells
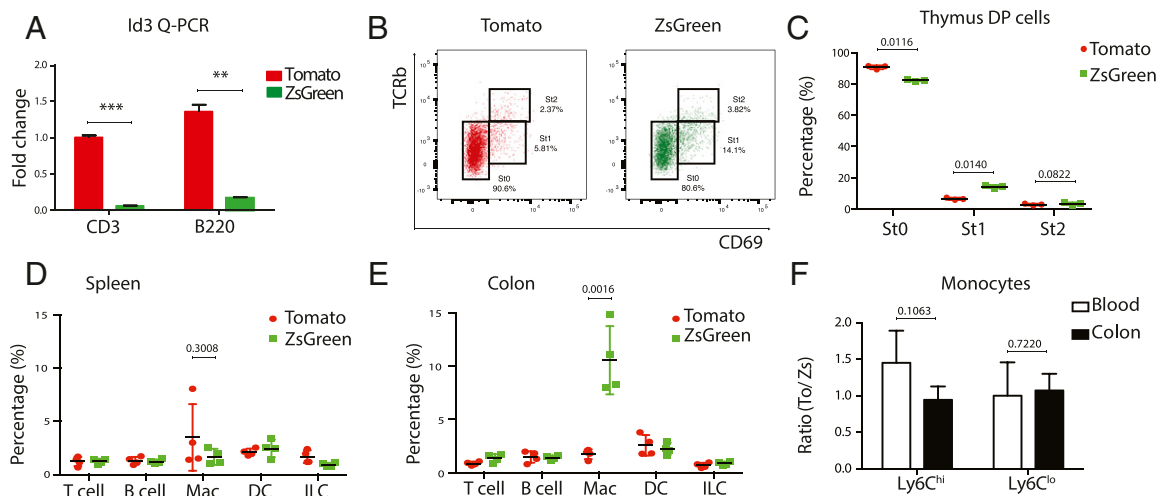

Fig. 2. Detection of cell-intrinsic functions of *Id3* in the analysis of *Id3* mosaic mice. (A) Q-PCR validation of *Id3* deletion in lineage-labeled CD3$^+$ T cells and B220$^+$ B cells. (B) Representative FACS plots of Tomato$^+$ and ZsGreen$^+$ CD4$^+$CD8$^+$DP thymocytes stained with CD69 and TCRβ markers. Cells are divided into three sequential developmental stages as shown with the St0, St1, and St2 gates. (C) Distributions of St0, St1, and St2 cells within double positive (DP) populations are compared between Tomato$^+$ and ZsGreen$^+$ groups. Each dot indicates the relative frequency of cells in the respective gate (B) from an individual mouse (n = 3, paired t test). (D and E) Analysis of lineage-positive T cells, B cells, macrophages, dendritic cells, and innate lymphoid cells in the spleen (D) and colon (E) of *Id3*-mosaic mice 1-y posttamoxifen treatment. Each point represents values seen in a single mouse (n = 4, paired t test). (F) Bar-graph summary of the Tomato$^+$/ZsGreen$^+$ ratio of Ly6C^{hi} and Ly6C^{lo} monocytes in the blood and colon lamina propria 6-mo posttamoxifen treatment (n = 3, paired t test).

located at the bottom of each crypt. Study with Confetti mice has demonstrated that any mosaicism introduced into the stem-cell pool will drift toward singularity with time due to competition among stem cells within each crypt (29). Indeed, we found that lineage-labeled crypt cells were converted from isolated patches at 1 wk into uniformly labeled entire crypts at 2 mo posttamoxifen treatment (Fig. 1E and *SI Appendix*, Fig. S2F). Thus, lineage tracing of the regeneration process of crypt epithelium with MASCOT produced a similar result as was reported with the Confetti mice (29).

Mosaic Analysis of Clonal Deletion of the *Id3* Gene. We next evaluated the effectiveness of MASCOT to induce mutant clones. We chose the *Id3^flox* conditional allele to compare the MASCOT method with conventional genetic methods, since the effect of *Id3* deletion on lymphopoiesis has been extensively characterized with both *Id3* germline (22, 30) and conditional knockout mice (31). After crossing *Cot2* and *R26^{F/Z}* reporters to the *Id3^{f/f}* background, mice were treated with tamoxifen to produce mosaic clones. ZsGreen$^+$ and Tomato$^+$ cells were detected at approximately equal frequency in myeloid, B, and T cells in the blood. Q-PCR analysis of *Id3* expression in sorted B and T cells confirmed the loss of *Id3* expression in ZsGreen$^+$ cells (Fig. 2A). A requirement for ID3 in T cell receptor-mediated positive selection has been demonstrated in the study of *Id3* germline or conditional knockout mice (22, 31). Therefore, we examined the relative frequency of *Id3*-mutant cells before, during, and immediately after positive selection based on CD69$^-$/TCRβ^{low} (St0), CD69$^+$/TCRβ^{low} (St1), and CD69$^+$/TCRβ^{hi} (St2) staining, respectively (Fig. 2B). A direct comparison between ZsGreen$^+$ cells and Tomato$^+$ cells showed that *Id3* deletion resulted in an increase in the frequency of St1 cells and corresponding decrease of St0 cells (Fig. 2C), indicating a development block during positive selection and a finding consistent with previous reports (22, 31). To gain a broader view of ID3 function in the development and homeostasis of hematopoietic cells, we examined lineage-labeled cells in secondary lymphoid organs and gut lamina propria 1-y posttamoxifen treatment. Lineage-labeled ZsGreen$^+$ or Tomato$^+$ cells were found at similar frequencies for most hematopoietic lineages examined, including myeloid cells, T cells, B cells, innate lymphoid cells, natural killer T cells, and T regulatory cells (Fig. 2 D and E and *SI Appendix*, Fig. S3 A and B). One exception observed in this study was gut macrophages, which exhibited a significant increase in the population size of ZsGreen$^+$ cells (Fig. 2E). Intestinal macrophages are a mixture of long-lived cells and newly replenished cells from circulating Ly6C$^+$ monocytes that migrate into the gut (32). To further determine whether the enrichment of lineage-labeled colonic macrophages is a result of developmental regulation or long-term homeostasis, we evaluated mosaic frequency of monocytes at the midpoint of year-long lineage tracking. Numbers of *Id3*-deficient ZsGreen$^+$ monocytes, both short-lived (Ly6C^{hi}) and long-lived (Ly6C^{lo}) either in blood or colon, were similar to those of their Tomato$^+$ wild-type counterparts (Fig. 2F and *SI Appendix*, Fig. S3C). Thus, the age-dependent accumulation of *Id3*-deficient ZsGreen$^+$ macrophages in colon is unlinked to ongoing replenishment of macrophages from circulating monocytes. It suggests that *Id3* deletion affects long-term homeostasis of preexisting tissue-resident macrophages in the gut. Collectively, our mosaic analysis of the *Id3* conditional allele illustrates the high sensitivity of the MASCOT method in detecting cell-intrinsic defects during development and long-term homeostasis.

Tracking Clonal Hematopoiesis in *Tet2* Mosaic Mice. Next, we tested MASCOT in CH induced by *Tet2* deletion, a phenomenon that has been well-established in both humans and mice (23). *Cot2;R26^{F/Z};-Tet2^{f/f}* mice were produced through intercross of parental lines *Cot2;R26^{F/F};Tet2^{f/f}* and *Cot2;R26^{Z/Z};Tet2^{f/f}*, where *Cot2* can be either homozygous or heterozygous. Deletion of *Tet2* among the

ZsGreen$^+$ cells upon tamoxifen treatment was verified by Q-PCR analysis of *Tet2* mRNA in flow cytometry-sorted splenic CD11b$^+$ myeloid cells (Fig. 3A). We then performed long-term tracking of lineage-labeled cells in a cohort of *Cot2;R26^{F/Z};Tet2^{f/f}* mice by periodic tail-vein bleeding. We found that the frequency of ZsGreen$^+$ cells in the blood rose gradually with age whereas the frequency of Tomato$^+$ cells remained stable (Fig. 3B and *SI Appendix*, Fig. S4). Parallel analysis of myeloid and lymphoid lineage cells also revealed differential impacts of *Tet2* deletion on different hematopoietic lineages. The frequency of *Tet2*-deficient clones was significantly higher in the myeloid compartment than in the lymphoid compartment after 30 wk of lineage tracking (Fig. 3C). Linear regression analysis of the growth curves within this time window further demonstrated differential impact of *Tet2* deletion on individual hematopoietic lineages (Fig. 3D). The expansion rates of lineage-tracked, *Tet2*-deficient myeloid, B, and T cells were 0.73, 0.23, and 0.08% per week, respectively. To determine whether mosaic frequency of blood lymphocytes reflected ongoing lymphopoiesis, we examined the frequency of *Tet2*-deficient T cells in the thymus and spleen. Lineage-labeled T cells in the thymus and spleen during this time window exhibited a similar change in frequency relative to the frequency of lineage-labeled myeloid cells as observed in the blood (Fig. 3E). We next examined clonal expansion in the bone marrow where myelopoiesis occurs. We found that clonal frequency of ZsGreen$^+$ cells was similar among HSC, lin$^-$cKit$^+$ progenitors, and CD11b$^+$ myeloid cells in the bone marrow (Fig. 3F and *SI Appendix*, Fig. S5). This result confirms that CH in *Tet2*-mosaic mice occurs in HSC and hematopoietic progenitors. Since the frequency of *Tet2*-deficient lymphocytes was significantly less than that of HSC and myeloid cells, we conclude that *Tet2*-deficient HSC promotes myelopoiesis while impairing lymphopoiesis. Collectively, our mosaic analysis confirmed the previous report of TET2 function in restricting HSC/myeloid expansion (11, 33, 34) and indicated a cell-intrinsic requirement of TET2 in lymphoid lineage development.

Mosaic Analysis of *Id3* and *Tet2* Double Mutations. To further examine the differential role of *Tet2* in regulating myelopoiesis versus lymphopoiesis, we sought to test whether *Tet2*-dependent lymphopoiesis could be further enhanced by a second mutation. In B cells, TET2 has been shown to directly interact with the E2A transcription factor, a key regulator of lymphopoiesis and the canonical target of ID3 (35). In addition, conditional deletion of *Tet2* and *Tet3* genes in T cells led to natural killer T cell lymphoma accompanied by an up-regulation of *Id3* (36). As reported in B cells (35), we found that TET2 and E2A also physically interact with each other in T cells (*SI Appendix*, Fig. S6). Thus, we tested the genetic interaction between *Tet2* and *Id3* in lymphopoiesis by generating and tracking *Tet2* and *Id3* double-deficient (DKO) mosaic clones in the blood (Fig. 4 A–C and *SI Appendix*, Fig. S7). Lineage tracking of ZsGreen$^+$ myeloid cells at 30-wk posttamoxifen treatment showed a similar degree of expansion between *Tet2/Id3* DKO mosaic mice and *Tet2* single-deficient (SKO) mosaic mice (Fig. 4D). In contrast, lineage tracing revealed a decrease in expansion of ZsGreen$^+$ B cells (Fig. 4E, P = 0.0002) and T cells (Fig. 4F, P = 0.006) in *Tet2/Id3* DKO mosaic mice over that of *Tet2* SKO mosaic mice. Linear regression analysis revealed that lineage-tracked DKO myeloid, B, and T cells expanded 0.66, 0.06, and 0.02% per week, respectively, within the first 32 wk posttamoxifen treatment (Fig. 4G). Based on the difference of observed expansion rates between SKO and DKO mosaic mice (*SI Appendix*, Fig. S8), we concluded that B and T cell development were further impaired after deletion of both the *Id3* and *Tet2* genes. Because B and T cell numbers were not altered in *Id3* mosaic mice (Fig. 2D), the severe impairment of lymphopoiesis in *Tet2/Id3* double-mosaic mice indicated a synergistic interaction between *Tet2* and *Id3* mutations in blocking lymphopoiesis. While further studies are
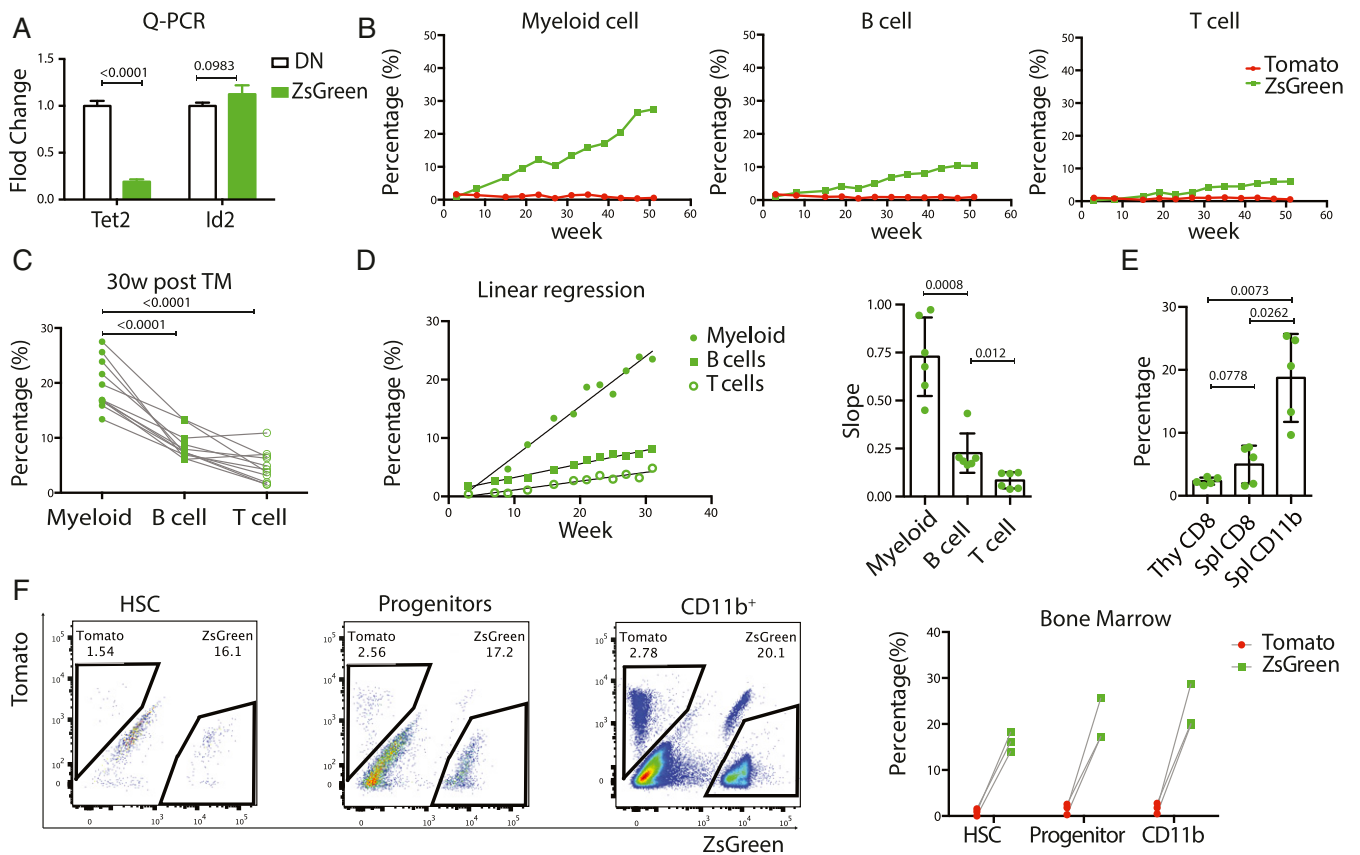
Fig. 3. Modeling clonal hematopoiesis with *Tet2* mosaic mice. (*A*) Q-PCR validation of *Tet2* deletion in ZsGreen-labeled CD11b^{+} myeloid cells posttamoxifen treatment of *Tet2*-mosaic mice (*n* = 4). *Id2* is included as a control. (*B*) Long-term tracing of lineage-positive cells in peripheral blood of *Tet2* mosaic mice. Representative longitudinal analysis of CD11b/c^{+} myeloid cells, CD19^{+} B cells, and CD3^{+} T cells from a single mouse is shown up to 51-wk posttamoxifen treatment. Graphs of additional mice are shown in *SI Appendix*, Fig. S4. (*C*) Clonal frequencies of ZsGreen[+] myeloid, B, and T cells are shown at 30-wk posttamoxifen treatment of *Tet2*-mosaic mice (*n* = 11). (*D*) Linear regression analysis of clonal frequency of ZsGreen[+] myeloid, B, and T cells in the first 32 wk posttamoxifen treatment for one representative mouse (*Left*) and bar-graph summary of slopes (*Right*) (*n* = 6, paired *t* test). (*E*) Comparison of clonal frequency between thymic CD8 T cells, splenic CD8 T cells, and splenic CD11b^{+} myeloid cells. Samples were collected between 6–9 mo posttamoxifen treatment (*n* = 5, paired *t* test). (*F*) Comparison of clonal frequency of lineage-positive HSC, lin⁻kit^{+} progenitors, and CD11b^{+} myeloid cells in the bone marrow of three *Tet2*-mosaic mice between 3.5–9-mo posttamoxifen treatment. (*Left*) Representative FACS plots of one mouse. (*Right*) Summary of three mice analyzed. FACS gating of HSC and lin⁻kit[+] progenitors are shown in *SI Appendix*, Fig. S5.

needed to determine whether this synergistic effect is caused by unchecked E2A activity in the absence of its interaction partners ID3 and TET2, the current finding demonstrates the feasibility of MASCOT for analysis of compound mutations.

Modeling Lymphomagenesis with MASCOT. In human studies, CH driven by *Tet2* mutations has been linked to the development of AML (1, 3, 4). However, a recent study of pediatric patients with germline *TET2* loss-of-function revealed development of lymphoma even though hematopoiesis of patient-derived stem cells displayed a skewing toward the myeloid lineage (37). We evaluated whether introduction of *Tet2* mosaicism at a young age could lead to either myeloid or lymphoid transformation at an older age in mice. We found that expansion of *Tet2*-deficient myeloid cells was tapered after 30-wk posttamoxifen treatment (Fig. 5*A*). Using Tomato^{+} cells as a reference, ZsGreen^{+} cells in myeloid, B cell, and T cell compartments all exhibited an increase from the beginning to the endpoint of lineage tracking (Fig. 5*B*). A comparison of percentages of ZsGreen^{+} cells between 30 wk and the endpoint of lineage tracking showed a significant increase of lineage-labeled B and T cells, but not myeloid cells, in this timeframe (Fig. 5*C*). After 1 y in lineage tracking, a significant number of mosaic mice exhibited myeloid expansion and an increase of B to T cell ratio (*SI Appendix*, Fig. S9 *A–C*). Upon dissection of mice at the age between 16–25 mo, we found 29% of *Tet2* single-mosaic

mice (4 out of 14) and 15% of *Tet2/Id3* double-mosaic mice (2 out of 13) exhibited splenomegaly and/or enlargement of lymph nodes (Fig. 5 *D* and *E* and *SI Appendix*, Fig. S9D). Histologic analysis also identified tumor masses in the liver (Fig. 5*F*). Fluorescent microscopy analysis of enlarged lymph nodes indicated high content of proliferating cells based on Ki67 staining and high content of *Tet2* mutant cells based on ZsGreen expression (Fig. 5*G*). Fluorescence-activated cell sorter (FACS) analysis further confirmed high content of ZsGreen^{+} B cells (Fig. 5*H*) and the blasting phenotype of the B cells in the enlarged lymph nodes (*SI Appendix*, Fig. S9E). These findings complement a recent report that conditional deletion of *Tet2* together with repeated immunization promotes B cell lymphomagenesis (38). However, many of our mosaic mice did not show tumor masses at the time of euthanasia even though they exhibited B cell expansion after 1 y of lineage tracking (*SI Appendix*, Fig. S9A). To test the possibility that the intact immune system in the mosaic mice suppresses malignant growth of the expanded B cells, we adoptively transferred splenocytes from two of the *Tet2/Id3* mosaic mice exhibiting B cell expansion but without visible tumor masses into *Rag2*-deficient mice. Although unfractionated splenocytes were used in the transfer, both donors demonstrated exclusive expansion of B cells in the *Rag2* hosts (Fig. 5 *I* and *J*), with development of aggressive lymphoma involving multiple organs, including liver and kidney (Fig. 5*K*). RNA analysis of tumor samples confirmed
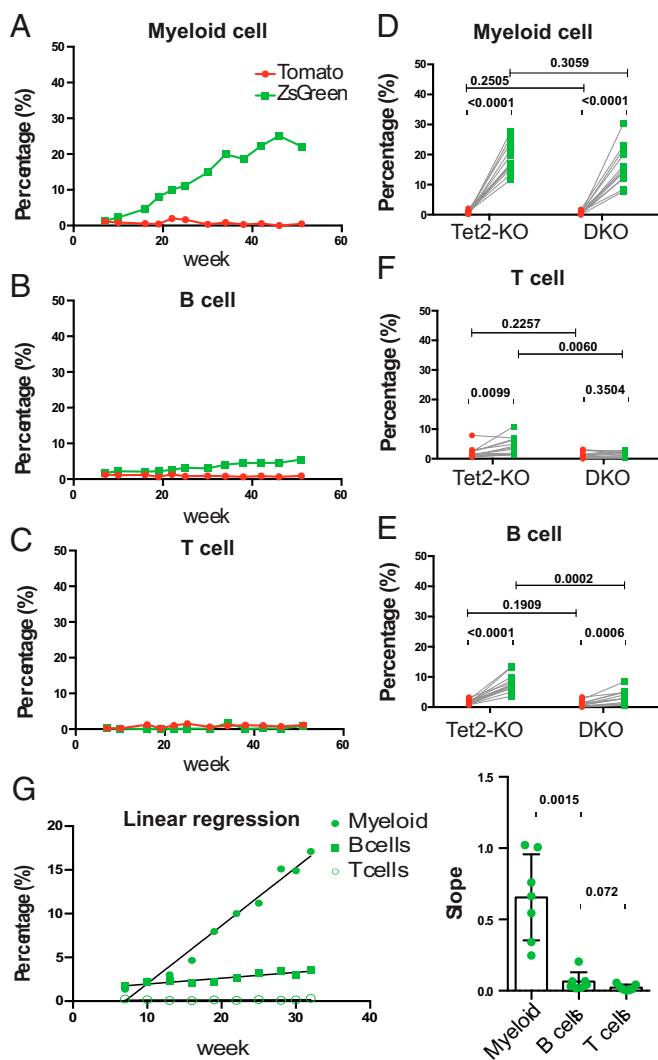
Wang et al.

Fig. 4. Mosaic analysis of *Tet2/Id3* double mutations. (*A–C*) Representative tracking graphs of lineage-positive cells in the *Tet2/Id3* mosaic mice during the first 51 wk posttamoxifen treatment. Graphs of additional mice are shown in *SI Appendix*, Fig. S7. (*D–F*) Comparison of percentages of lineage-labeled cells at 30-wk posttamoxifen treatment of *Tet2* SKO (*n* = 13) and *Tet2/Id3* DKO (*n* = 12) mosaic mice. *t* tests are paired between Tomato⁺ cells and ZsGreen⁺ cells within each genotype group and unpaired between genotype groups. (*G*) Linear regression analysis of ZsGreen⁺ cell expansion in the first 32 wk post tamoxifen treatment (as described in Fig. 3*F*). (*Left*) Representative plot for one DKO mouse. (*Right*) Bar-graph summary of slopes for myeloid, B, and T cells (*n* = 7, paired *t* test).

the loss of *Tet2* expression (*SI Appendix*, Fig. S10). Thus, CH initiated with *Tet2* deletion in young adult mice leads to lymphoid proliferative phenomenon and stochastic transformation into *Tet2*-deficient lymphoma at older ages.

Discussion

Our mosaic analysis of *Id3* and *Tet2*, either individually or in combination, demonstrated the utility of the MASCOT method in identifying cell-intrinsic gene function in the contexts of lineage development and long-term homeostasis. The use of a separate marker to label a reference population represents an improvement over the MASTR method. In comparison with the MADM method which requires mitosis to produce differentially labeled daughter clones (17), MASCOT can produce mosaic clones in both mitotically active (e.g., blood and epithelium) and

quiescent tissues (e.g., muscle). Although the ratio between Tomato-labeled cells and ZsGreen-labeled cells is stochastically determined based on the binary outcomes of Flp/FRT-mediated recombination, it is fixed upon completion of tamoxifen treatment in any given animal. Thus, any changes in the relative ratio among sister lineages at different timepoints during longitudinal tracking would provide a sensitive readout for cell-intrinsic functions. In addition to confirming previous observations relating to the roles of *Id3* and *Tet2* in lymphopoiesis and clonal hematopoiesis, the MASCOT method enabled us to: 1) uncover a cell-intrinsic function of *Id3* in regulating homeostasis of gut-resident macrophages; 2) define differential roles of *Tet2* in myeloid vs. lymphoid lineage development; 3) analyze genetic interaction between *Id3* and *Tet2* in lymphopoiesis; and 4) establish a lymphoma model based on long-term progression from CH. Thus, MASCOT provides a useful genetic tool for dissecting cell-intrinsic phenotypes in developmental and cancer studies.

The mosaic analysis described here allowed us to simulate a broader window of CH driven by *Tet2* deletion, from the initial expansion of mutation cells at a very young age to lymphoma development at much older ages. It is important to point out that mutations generated in the MASCOT mice involve a small number of cells whereas most CH are a result of clonal expansion from a single mutant. Despite this, at the population level, our study revealed that *Tet2* deletion promoted expansion of the myeloid compartment, an outcome consistent with the role of TET2 in restricting HSC expansion demonstrated using the bone marrow chimeric approach (11, 33, 34). Our model also indicates that although *Tet2* deletion initially suppresses lymphoid expansion, it promotes lymphomagenesis at a later stage. Previous studies of *Tet2* germline knockout mice have observed high frequency of myeloid malignancies (39) and human chronic myelomonocytic leukemia-like disease (11). More recent study of B-lineage-specific *Tet2* knockout reported *Tet2*-deficient B cell lymphoma in aged mice (38, 40). An important difference between our MASCOT mouse model and these other *Tet2*-knockout studies is the presence of an intact immune system in our *Tet2*-mosaic mice. The relatively low frequency of tumor incidence observed in our *Tet2*-mosaic mice suggests that an active immune surveillance is still in place even after an overt myeloid and lymphoid expansion. Thus, the MASCOT method could potentially be used as an immunocompetent model for preclinical investigation of lymphomagenesis and lymphoma treatment.

The current application of MASCOT relies on $R26^{FlpoER}$ to induce mosaicism at low frequency in nearly all tissue types and thus offers broad applications. While the study presented here focused on hematopoietic system, mosaic mice created by MASCOT may also be used for examining cell-intrinsic function in other organs, such as the colon (Fig. 1*E*), where lineage-marked colon epithelial clones are readily detectable with fluorescent microscopy. In comparison to the widely used CreER or MxCre system (15, 16), MASCOT adds an internal reference population that allows more accurate quantification of any change in clonal size within the same tissue. On the flip side, the current version of the MASCOT design requires more rounds of breeding than the inducible CreER and MxCre systems for experimental execution. Therefore, the latter ones would be the first choice in experiments when the goal is simply to generate lineage-marked mutant cells. The burden of multiple rounds of breeding associated with MASCOT could be reduced in the future by engineering MASCOT and $R26^{FlpoER}$ into the same locus. Another difference between the inducible Cre systems and our MASCOT systems is that Cre is transiently expressed in the inducible system and constitutively expressed in the mosaic analysis among mutant cells generated. One cannot rule out the possibility that Cre-associated toxicity may interfere with experimental readout. Therefore, it is critical to test the mosaic analysis system

Fig. 5. Lymphomagenesis in *Tet2* and *Tet2/Id3* mosaic mice after long-term tracking. (*A*) Representative lineage tracking of a *Tet2* single and a Tet2/Id3 double-knockout mosaic mouse that underwent abrupt B cell expansion after long-term lineage tracking. (*B*) Tomato+ and ZsGreen+ cells in myeloid, B, and T cell compartments of *Tet2* SKO mosaic mice are independently calculated as fold changes between the beginning (<1 mo) and the endpoint (>16 mo) of lineage tracking (*n* = 9, paired *t* test). (*C*) Comparison of labeling frequency of ZsGreen+ cells between 30 wk and the endpoints (over 16 mo) of lineage tracking (same group as in *B*, *n* = 9, paired *t* test). (*D*) Gross phenotypes observed in 6 mice out of 27 mice upon euthanasia. (*E*) Representative gross phenotypes of spleen are shown for a *Tet2* SKO and a *Tet2/Id3* DKO mosaic mouse in comparison with the spleen of a nonmosaic control mouse (*Left*). (*F*) Liver with white nodules was sectioned and stained with H&E (hematoxylin and eosin), with the insert showing a border area between lymphocytes and hepatocytes (red arrow). (*G*) Immunofluorescent image of a frozen section from an enlarged lymph node analyzed for ZsGreen (*Left*) and Ki67 expression (*Right*). DAPI channel is included in the Ki67 image. (*H*) Representative FACS analysis of myeloid (CD11b+) and B (B220+) cells in the blood and spleen of a mouse with tumors (*n* = 6). (*I* and *J*) Blood tracking after adoptive transfer of total splenocytes from two independent mosaic donors (recipients *n* = 7). Total B and T cell count (*I*) and lineage frequency of B cells (*J*) were tracked for 21 wk before terminal analysis when the mice became visibly sick. (*K*) H&E staining of tumor infiltrates in the liver and kidney at 21 wk.

on the wild-type background prior to using it in the mosaic analysis of mutant clones. One more caveat of using $R26^{FlpoER}$ is that dominant clones arising in one cell lineage may interfere with mosaic analysis of other cell types in the same mice, particularly during long-term tracing of tumorigenesis. In our study of *Tet2* mosaic mice, the fast-growing tumor types may prevent further study of other tumor types that develop in a slower pace. This issue could be addressed in the future by combining MASCOT with lineage-specific FlpoER strains that restrict mosaic analysis to designated tissue types.

In summary, the MASCOT method enables easy tracking and retrieving of mutant cells from different tissues at any point during lineage tracking for quantitative assessment of cell-intrinsic phenotypes. With a large number of loxP-based conditional strains already produced in the field, MASCOT-based mosaic analysis provides another valuable tool to aid functional dissection of somatically acquired mutations in studies of development and disease.

Methods

Animal Procedures.

Mouse strains and housing. The MASCOT reporter strain was produced in the Duke Transgenic Mouse Facility. The $Tet2^f$ conditional allele (Jax mice # 017573 $Tet2^{tm1.1Iaai}$), the $R26^{ZsGreen}$ reporter (Jax mice # 007906, also known as Ai6), and the $Flpo^{ER}$ strain (Jax mice # 019016) were purchased from the Jackson Laboratory. The *Id3* conditional allele (31) was maintained in our breeding colony. All experimental mice were housed and bred in SPF barrier facilities managed by the Division of Laboratory Animal Research at Duke University. Animal protocols for the reported studies were reviewed and approved by Duke University Institutional Animal Care and Use Committee.

Modification of the $R26^{ZsGreen}$ strain. The original $R26^{ZsGreen}$ strain contains a pair of FRT sites flanking the reporter, in addition to the flox-stop cassette placed between the CAG promoter and ZsGreen (*SI Appendix*, Fig. S2A). To avoid inadvertent deletion of the ZsGreen by Flp-mediated recombination, we mutated the downstream FRT site with Crispr-CAS9–aided targeting. Transgenic lines were established at the Duke Transgenic Mouse Facility by microinjection of the guide RNA and CAS9 constructs into fertilized embryos. One of the modified alleles, named $R26^{Z10}$, was established and used in this study.

Blood tracking of mosaic clones. Approximately 10 µL of blood were collected from tail vein by bleeding with a 21-gauge needle at a frequency no more than once per week. Leukocytes were analyzed on either Canto or FortessaX20 (BD) flow cytometer after lysing red blood cells and staining the remaining cells with anti-CD45, B220, CD19, CD11b, CD11b, and CD3 antibodies in a single tube using multiple color analysis.

Adoptive transfer. Spleens from donor mice were mechanically dissociated into single-cell suspensions and treated with red blood cell lysing buffer. After washing with 1× phosphate-buffered saline (PBS) twice, live nucleated cells were counted and resuspended at 2.5×10^7 cell/mL in 1× PBS. 5×10^6 cells in 200 µL was transferred into each $Rag2^{-/-}$ mouse via tail-vein injection.

Immunofluorescence Microscopy. Tissues were fixed in 4% paraformaldehyde for 24 h, dehydrated in 30% sucrose for 24 h, embedded and frozen in OCT cutting compound, and then cut into 8-µm frozen sections. Primary antibody anti-B220 (Abcam ab64100) and anti-Ki67 (Abcam ab15580) were incubated at 4 °C for 24 h and then washed three times with 1× PBS. Slides were incubated with the secondary antibodies Alexa Fluor 647-conjugated goat anti-rat (eBioscience, A-21247) and goat anti-rabbit antibody (Invitrogen, A32733) for 24 h at 4 °C in dark. After washing for three times, the slides were mounted with DAPI-containing mounting medium (VECTORLAB, H-1200). Images were collected with a Zeiss Axio imager.

Q-PCR. Splenocytes were stained with anti-CD3, anti-B220, and anti-CD11b antibodies before sorting for Tomato⁺, ZsGreen⁺, or double-negative populations. Cell pellets were lysed with TRIzol (Invitrogen, 15596018), RNA was isolated with Zymo Direct-zol RNA Kits (Zymo Research, 2050), and cDNA was prepared with SuperScript III CellsDirect cDNA Synthesis Kit (Invitrogen, 18080200). Fast SYBR Green kits (Thermo, 4385612) were used for Q-PCR reactions. Primers were Tet2_F: agagcctcaagcaaccaaaa; Tet2_R: acatccctgaga-gctcttgc. Id2_F: cgacccgatgagtctgctcta; Id2_R: gacgatagtgggatgcgagtc. Id3_F: agcttttgccactgaccc; Id3_R: agatcgaagctcatccatgc.

Isolation of Intestinal Lamina Propria Lymphocytes. The colon was dissected free of the fat and connective tissue, cut open longitudinally, washed clean, and cut into 1-cm small pieces. Intraepithelial lymphocytes were removed by washing with ethylenediaminetetraacetic acid (EDTA)-containing buffer twice for 10 min each. The resulting tissue was digested in prewarmed Collagenase VIII (Sigma, C2139) and DNase I (Sigma, DN25) buffer at 37 °C for 50 min. Lamina propria lymphocytes were isolated with 40 and 80% Percoll (Sigma, GE17-0891-01), and stained with a mixture of lineage antibodies (CD45, CD90, CD3, CD24, CD11b, CD11c, F4/80, CD64, MHCII) for final analysis on a flow cytometer (FortessaX20, BD).

Data Availability. All study data are included in the article and *SI Appendix*.

1. M. Xie et al., Age-related mutations associated with clonal hematopoietic expansion and malignancies. *Nat. Med.* **20**, 1472–1478 (2014).
2. T. McKerrell et al.; Understanding Society Scientific Group, Leukemia-associated somatic mutations drive distinct patterns of age-related clonal hemopoiesis. *Cell Rep.* **10**, 1239–1245 (2015).
3. G. Genovese et al., Clonal hematopoiesis and blood-cancer risk inferred from blood DNA sequence. *N. Engl. J. Med.* **371**, 2477–2487 (2014).
4. S. Jaiswal et al., Age-related clonal hematopoiesis associated with adverse outcomes. *N. Engl. J. Med.* **371**, 2488–2498 (2014).
5. S. Abelson et al., Prediction of acute myeloid leukaemia risk in healthy individuals. *Nature* **559**, 400–404 (2018).
6. P. Desai et al., Somatic mutations precede acute myeloid leukemia years before diagnosis. *Nat. Med.* **24**, 1015–1023 (2018).
7. S. Jaiswal, B. L. Ebert, Clonal hematopoiesis in human aging and disease. *Science* **366**, eaan4673 (2019).
8. M. Zhu et al., Somatic mutations increase hepatic clonal fitness and regeneration in chronic liver disease. *Cell* **177**, 608–621.e12 (2019).
9. I. Martincorena et al., Tumor evolution. High burden and pervasive positive selection of somatic mutations in normal human skin. *Science* **348**, 880–886 (2015).
10. I. Martincorena et al., Somatic mutant clones colonize the human esophagus with age. *Science* **362**, 911–917 (2018).
11. K. Moran-Crusio et al., Tet2 loss leads to increased hematopoietic stem cell self-renewal and myeloid transformation. *Cancer Cell* **20**, 11–24 (2011).
12. G. A. Challen et al., Dnmt3a is essential for hematopoietic stem cell differentiation. *Nat. Genet.* **44**, 23–31 (2011).
13. R. Shrestha et al., Molecular pathogenesis of progression to myeloid leukemia from TET-insufficient status. *Blood Adv.* **4**, 845–854 (2020).
14. O. Mansier et al., Description of a knock-in mouse model of JAK2V617F MPN emerging from a minority of mutated hematopoietic stem cells. *Blood* **134**, 2383–2387 (2019).
15. R. Kühn, F. Schwenk, M. Aguet, K. Rajewsky, Inducible gene targeting in mice. *Science* **269**, 1427–1429 (1995).
16. D. Metzger, J. Clifford, H. Chiba, P. Chambon, Conditional site-specific recombination in mammalian cells using a ligand-dependent chimeric Cre recombinase. *Proc. Natl. Acad. Sci. U.S.A.* **92**, 6991–6995 (1995).
17. H. Zong, J. S. Espinosa, H. H. Su, M. D. Muzumdar, L. Luo, Mosaic analysis with double markers in mice. *Cell* **121**, 479–492 (2005).
18. Z. Lao, G. P. Raju, C. B. Bai, A. L. Joyner, MASTR: A technique for mosaic mutant analysis with spatial and temporal control of recombination using conditional floxed alleles in mice. *Cell Rep.* **2**, 386–396 (2012).
19. L. Sun, X. Wu, M. Han, T. Xu, Y. Zhuang, A mitotic recombination system for mouse chromosome 17. *Proc. Natl. Acad. Sci. U.S.A.* **105**, 4237–4241 (2008).
20. C. Liu et al., Mosaic analysis with double markers reveals tumor cell of origin in glioma. *Cell* **146**, 209–221 (2011).
21. Y. Zhu et al., Generation of Dhx9-deficient clones in T-cell development with a mitotic recombination technique. *Genesis* **50**, 543–551 (2012).
22. R. R. Rivera, C. P. Johns, J. Quan, R. S. Johnson, C. Murre, Thymocyte selection is regulated by the helix-loop-helix inhibitor protein, Id3. *Immunity* **12**, 17–26 (2000).
23. C. J. Lio, H. Yuita, A. Rao, Dysregulation of the TET family of epigenetic regulators in lymphoid and myeloid malignancies. *Blood* **134**, 1487–1497 (2019).
24. D. P. Steensma et al., Clonal hematopoiesis of indeterminate potential and its distinction from myelodysplastic syndromes. *Blood* **126**, 9–16 (2015).
25. S. Turan, J. Kuehle, A. Schambach, C. Baum, J. Bode, Multiplexing RMCE: Versatile extensions of the Flp-recombinase-mediated cassette-exchange technology. *J. Mol. Biol.* **402**, 52–69 (2010).

GENETICS

26. A. Alexandrov, M. D. Shu, J. A. Steitz, Fluorescence amplification method for forward genetic discovery of factors in human mRNA degradation. *Mol. Cell* **65**, 191–201 (2017).
27. S. Ding *et al*., Efficient transposition of the piggyBac (PB) transposon in mammalian cells and mice. *Cell* **122**, 473–483 (2005).
28. L. Madisen *et al*., A robust and high-throughput Cre reporting and characterization system for the whole mouse brain. *Nat. Neurosci.* **13**, 133–140 (2010).
29. H. J. Snippert *et al*., Intestinal crypt homeostasis results from neutral competition between symmetrically dividing Lgr5 stem cells. *Cell* **143**, 134–144 (2010).
30. L. Pan, S. Sato, J. P. Frederick, X. H. Sun, Y. Zhuang, Impaired immune responses and B-cell proliferation in mice lacking the Id3 gene. *Mol. Cell. Biol.* **19**, 5969–5980 (1999).
31. Z. Guo *et al*., Modeling Sjögren's syndrome with Id3 conditional knockout mice. *Immunol. Lett.* **135**, 34–42 (2011).
32. F. Ginhoux, M. Guilliams, Tissue-resident macrophage ontogeny and homeostasis. *Immunity* **44**, 439–449 (2016).
33. M. Ko *et al*., Ten-eleven-translocation 2 (TET2) negatively regulates homeostasis and differentiation of hematopoietic stem cells in mice. *Proc. Natl. Acad. Sci. U.S.A.* **108**, 14566–14571 (2011).
34. C. Quivoron *et al*., TET2 inactivation results in pleiotropic hematopoietic abnormalities in mouse and is a recurrent event during human lymphomagenesis. *Cancer Cell* **20**, 25–38 (2011).
35. C. W. Lio *et al*., Tet2 and Tet3 cooperate with B-lineage transcription factors to regulate DNA modification and chromatin accessibility. *eLife* **5**, e18290 (2016).
36. A. Tsagaratou *et al*., TET proteins regulate the lineage specification and TCR-mediated expansion of iNKT cells. *Nat. Immunol.* **18**, 45–53 (2017).
37. J. Stremenova Spegarova *et al*., Germline TET2 loss-of-function causes childhood immunodeficiency and lymphoma. *Blood* **136**, 1055–1066 (2020).
38. P. M. Dominguez *et al*., TET2 deficiency causes germinal center hyperplasia, impairs plasma cell differentiation, and promotes B-cell lymphomagenesis. *Cancer Discov.* **8**, 1632–1653 (2018).
39. Z. Li *et al*., Deletion of Tet2 in mice leads to dysregulated hematopoietic stem cells and subsequent development of myeloid malignancies. *Blood* **118**, 4509–4518 (2011).
40. E. Mouly *et al*., B-cell tumor development in *Tet2*-deficient mice. *Blood Adv.* **2**, 703–714 (2018).